

1
2 **Laminar Segregation of Sensory Coding and Behavioral**
3 **Readout in Macaque V4**

4
5
6 **Warren W. Pettine¹, Nicholas A. Steinmetz², Tirin Moore**

7
8
9 **Department of Neurobiology and Howard Hughes Medical Institute, Stanford**
10 **University School of Medicine, Stanford CA 94305**

11
12
13 **Correspondence to:**
14 **Tirin Moore**
15 **Department of Neurobiology, Fairchild Bldg., Campus Drive West**
16 **Stanford University, Stanford CA, 94305**

17
18
19
20 **1,975 Words (main text)**
21 **3 Figures**

22
23 1. Current address: Center for Neural Science, New York University, 4 Washington Pl
24 #809, New York, NY 10003

25 2. Current address: University College, London, The Cruciform Building, Gower Street,
26 London WC1E 6AE

27
28
29 **Acknowledgements.**

30 This work was supported by NEI grant EY014924 to T.M., a National Science
31 Foundation graduate fellowship to N.A.S., and an HHMI medical research fellowship to
32 W.W.P. We thank S. Hyde for valuable assistance with animal care, and B. Schneeweis
33 for designing and building the 3D electrode angler.

34
35

36
37

38 **Summary**

39 Neurons in sensory areas of the neocortex are known to represent information both about
40 sensory stimuli and behavioral state, but how these two disparate signals are integrated across
41 cortical layers is poorly understood. To study this issue, we measured the coding of visual
42 stimulus orientation and of behavioral state by neurons within superficial and deep layers of
43 area V4 in monkeys while they covertly attended or prepared eye movements to visual stimuli.
44 We show that single neurons and neuronal populations in superficial layers convey more
45 information about the orientation of visual stimuli, whereas single neurons and neuronal
46 populations in deep layers convey greater information about the behavioral relevance of those
47 stimuli. In particular, deep layer neurons encode greater information about the direction of
48 prepared eye movements. These results reveal a division of labor between laminae in the
49 coding of visual input and visually guided behavior.

50
51
52
53

54 Introduction

55 Visual area V4 comprises an intermediate processing stage in the primate visual hierarchy^{1,2}.
56 V4 neurons exhibit selectivity to color^{3,4}, orientation^{5,6}, and contour^{7,8}, and appear to be
57 segregated according to some of these properties across the cortical surface⁹. Distinct from
58 their purely sensory properties, V4 neurons are also known to encode information about
59 behavioral and cognitive factors, particularly covert attention¹⁰, but also reward value¹¹, and the
60 direction of planned saccadic eye movements¹²⁻¹⁴. As with other neocortical areas, V4 is
61 organized by a characteristic laminar structure, in which granular Layer 4 neurons receive
62 feedforward sensory input from hierarchically 'lower' visual cortical areas, namely area V1 and
63 V2^{1,15-17}. Projections from area V4 to hierarchically 'higher' visual areas, such as TEO and
64 posterior inferotemporal (IT) cortex, originate largely from layers II-III^{1,18}, whereas layer 5
65 neurons project back to V1 and V2 and subcortically to the superior colliculus¹⁸⁻²⁰.

66 Recent studies have found laminar differences in attention-related modulation of neural
67 activity. Buffalo et al., (2011)²¹ observed that changes in LFP power due to the deployment of
68 covert attention differed between superficial and deep layers; gamma-band increases were
69 found in superficial layers and alpha-band decreases were found in deep layers. Increases in
70 firing rate with attention were observed to be similar in both laminar divisions. Nandy et al.
71 (2017)²² compared attention-driven changes in spiking activity across three laminar
72 compartments of V4 and observed significant firing rate modulation in superficial, granular and
73 deep layers. In addition, they observed subtle, but reliable, differences in other aspects of
74 activity across layers (e.g. spike count correlations). However, no previous studies have
75 compared stimulus tuning properties, or looked for differences in other types of behavioral
76 modulation across layers.

77 To investigate the layer dependence of stimulus and behavioral modulation in area V4,
78 we measured the selectivity of V4 neurons to both factors in monkeys performing an attention-

79 demanding task that dissociated covert attention from eye movement preparation. We then
80 compared orientation tuning and behavioral modulation in superficial and deep layer individual
81 units, and populations.

82

83 **Results and Discussion**

84 Two monkeys (G and B) were trained to perform an attention-demanding task²³ that required
85 them to detect orientation changes in one of four peripheral oriented grating stimulus patches
86 while maintaining central fixation (Figure 1a; see Experimental Procedures)¹². Upon detection of
87 a change, monkeys were rewarded for saccadic eye movements to the patch opposite the
88 orientation change. Both monkeys performed well above chance. We recorded the activity of
89 698 units (277 single-units and 421 multi-units) at 421 sites using 16-channel linear array
90 electrodes while monkeys performed the task. Electrodes were delivered perpendicular, or
91 nearly perpendicular, to the cortical surface as guided by magnetic resonance imaging, and
92 confirmed by receptive field (RF) alignment (Figure 1b). In each recording session, data from
93 the 16 electrode channels were assigned laminar depths, relative to a common current source
94 density (CSD) marker (Figure 1c, see Methods).

95

96 **Orientation Selectivity**

97 We first examined the proportion of units exhibiting significant orientation tuning and compared
98 that proportion across layers (see Methods). Overall, 63.75% (445/698; $P < 0.001$) of units were
99 significantly tuned for stimulus orientation (Figure 2a). Of these, we found that a significantly
100 higher proportion of superficial units (74.9%) were tuned compared to deep units (58.3%; Chi-
101 squared, $P = 9.7 \times 10^{-6}$). Next, we fit Gaussian functions to the normalized mean firing rates
102 elicited by the eight orientations for each of the 698 units (Figure 2b, see Methods). Across
103 superficial and deep layers, 35.5% (248) of units were well-fit ($R^2 > 0.7$). Among the well-fit

104 units, 98 were recorded in superficial layers (36.6% of superficial units) and 150 were recorded
105 in deep layers (35% of deep neurons). These proportions were not significantly different from
106 each other (Chi-squared, $P > 0.05$). Comparing fit parameters, we observed no significant
107 differences in width or baseline between superficial and deep layers (width, superficial = 0.84,
108 deep = 0.67, $P > 0.05$; baseline, superficial = 0.10, deep = 0.10, $P > 0.05$). However, the mean
109 amplitude of superficial layer units was significantly greater than that of deep layer units
110 (superficial = 0.17; deep = 0.13; $P = 0.0179$).

111 Measurements of orientation tuning in individual units indicate that superficial layer units
112 in our dataset were better tuned to stimulus orientation than their deep layer counterparts.
113 However, we considered that these measurements might not capture all of the information
114 conveyed about stimulus orientation. We therefore took a population decoding approach²⁴ to
115 measure the information available about orientation in the activity of all units within superficial or
116 deep layers (see Methods). Decoder performance was computed as a function of neuronal
117 population size. We then fit a “neuron-dropping” curves (NDCs)²⁵ to the values, and compared
118 the confidence intervals of the fit parameters for slope (b) and asymptote (c) for superficial and
119 deep populations. Both superficial and deep units performed significantly above chance for all
120 population sizes greater than zero. The NDS curve for superficial populations had a significantly
121 greater slope (superficial $b = 0.03071$, 95% CI: 0.03002, 0.0314; deep $b = 0.01976$, 95% CI:
122 0.01925, 0.02026), and asymptotic performance was about 7% higher than deep units
123 (superficial, $c = 0.9622$, 95% CI: 0.9597, 0.9647; deep, $c = 0.8969$, 95% CI: 0.8931, 0.9008).
124 Thus, as with the single-unit analysis, we found that stimulus orientation was more accurately
125 encoded by populations of superficial layer neurons.

126 The robust differences in orientation selectivity we observed between the superficial and
127 deep layer units raise important questions, such as whether those differences result simply from
128 the known compartmentalization of orientation versus color tuning across V4⁹. However, even if
129 we had oversampled one compartment or the other (e.g. more color compartments), doing so

130 would not be expected to introduce an overall bias between upper and lower layers. It is also
131 worth noting that since the primary evidence of feature-specific compartments in V4 comes from
132 optical imaging, where much of the signal derives from superficial layers²⁶, those compartments
133 may be less well-defined within infragranular layers. Indeed, anatomical evidence indicates that
134 intrinsic horizontal connections in V4, which appear to reciprocally connect columns across
135 millimeters of cortex, exist predominantly in superficial layers, similar to earlier (e.g., V1, V2)
136 and later stages of visual cortex²⁷.

137 Second, our results raise the important question of whether the selectivity to other
138 features, e.g. color or contour, is also greater in superficial layers. For example, substantial
139 previous evidence suggests that neurons in V4 are unique in the computation of stimulus
140 contour, not orientation, the former deriving from the orientation-specific input they receive from
141 V1 and V2^{7,8,28,29}. In such a case, our observations within orientation selectivity might not
142 generalize to all other types of selectivity. Instead, the results might only generalize to features
143 computed at earlier stages. Nonetheless, our results reveal the importance of assessing the
144 laminar dependence of stimulus selectivity across visual cortex.

145

146 **Coding of Eye Movement Preparation and Covert Attention**

147 We next examined activity across superficial and deep layers when monkeys covertly attended
148 the visual stimulus, prepared a saccade to that stimulus, or ignored it. We first compared the
149 average modulation for individual neuronal recordings made at varying laminar depths aligned
150 to the superficial/deep boundary (Figure 3A). Overall, modulation across depth was significantly
151 greater during eye movement preparation than during covert attention ($P = 0.0024$), a result we
152 reported previously¹⁰. However, we observed no significant main effect of depth ($P > 0.05$), or
153 an interaction of attention type and depth ($P > 0.05$). Nonetheless, movement-related
154 modulation appeared to peak within the deep layers, suggesting that the difference in attention
155 type was due to greater eye movement modulation in those layers. Thus, we directly compared

156 the magnitude of modulation in the two attention types collapsed within superficial or deep
157 layers. This revealed that while there was no significant difference in modulation in superficial
158 layers ($P > 0.05$), saccade modulation was significantly greater within deep layers ($P = 0.0041$).

159 Next, as with stimulus orientation, we decoded the behavioral condition using population
160 activity from superficial (277 units) or deep (419 units) layers (Figure 3b), and classified activity
161 as occurring during covert attention, saccade preparation, or control trials. The performance of
162 decoding deep populations was significantly greater than superficial at all populations of >30
163 units. Although the slopes of the NDS fits were not significantly different, (superficial $b =$
164 0.01918 , 95% CI: 0.01842 , 0.01993 ; deep $b = 0.01849$, 95% CI: 0.01773 , 0.01925), the
165 asymptotic performance for deep units exceeded that of superficial units by more than 5%
166 (superficial, $c = 0.6073$, 95% CI: 0.6053 , 0.6092 ; deep, $c = 0.6534$, 95% CI: 0.6509 , 0.6559).
167 Thus, the behavioral condition was more accurately encoded by populations of deep layer units.

168 To investigate the conditions driving performance, we then conducted pairwise decoding
169 of attentional conditions (Figure 3c). When decoding covert attention versus control, we found
170 that although the NDC slope for deeper populations was greater than that of superficial
171 populations, (superficial $b = 0.01974$, 95% CI: 0.01882 , 0.02066 ; deep $b = 0.02671$, 95% CI:
172 0.0255 , 0.02792), asymptotic performances were not significantly different (superficial, $c =$
173 0.7565 , 95% CI: 0.7544 , 0.7586 ; deep, $c = 0.758$, 95% CI: 0.7564 , 0.7596). In decoding
174 saccade preparation versus covert attention, we found a greater slope for superficial layer units,
175 (superficial $b = 0.01739$, 95% CI: 0.01646 , 0.01832 ; deep $b = 0.01446$, 95% CI: 0.01361 ,
176 0.01531), but a greater asymptotic performance for deep layer populations (superficial, $c =$
177 0.7475 , 95% CI: 0.7448 , 0.7503 ; deep, $c = 0.7785$, 95% CI: 0.7745 , 0.7825). Lastly, when
178 decoding saccade preparation versus control, we found that although the slopes were not
179 significantly different, (superficial $b = 0.02765$, 95% CI: 0.02639 , 0.02891 ; deep $b = 0.0286$,
180 95% CI: 0.02714 , 0.03006), the asymptotic performance was $\sim 3\%$ greater for deep units
181 (superficial, $c = 0.7295$, 95% CI: 0.7282 , 0.7308 ; deep, $c = 0.7651$, 95% CI: 0.7634 , 0.7668).

182 Thus, coding of attentional state, covert or overt, was greatest for units in the deep layers,
183 where eye movement preparation was most strongly encoded.

184 Few studies have examined the influence of motor preparation on the responses of
185 neurons in visual cortex, yet it is nonetheless clear that visually driven activity is affected by
186 impending eye movements at many stages of the primate visual system^{30–33}. Moreover, we have
187 shown previously¹², and in the present study, that the movement-related modulation of V4
188 activity is not only dissociable from modulation by covert attention, but it is more reliable. Those
189 findings are consistent with the hypothesis that visual cortical areas contribute directly to visually
190 guided saccades, particularly the refinement of saccadic plans according to features coded by
191 particular visual areas (e.g. shape in area V4)^{34–36}.

192 Our observation of stronger eye movement-related modulation in deep layers is also
193 consistent with the fact that projections to the superior colliculus emanate principally from layer
194 V pyramidal neurons throughout extrastriate visual cortex³⁷. Moreover, deep layer neurons are
195 a major source of feedback projections¹, and thus the relative robustness of behavioral signals
196 within deep layers may reflect the projection of those signals to earlier stages of visual
197 processing. Consistent with this notion, a previous study of attentional effects in areas V1, V2
198 and V4 found evidence of a “backward” progression of modulation in these areas that begins in
199 V4 and proceeds to V1²¹. Thus, the unique contributions of deep layer neurons to oculomotor
200 output and in top-down influences may account for their superior coding of behavioral variables.

201

202 **Conclusion**

203 We observed significantly greater orientation selectivity among units within the superficial layers
204 of V4 using both tuning measures in single neurons and decoding of population activity. In
205 contrast, using both single-unit and population activity, we observed that deeper layers
206 conveyed more information about the behavioral relevance of visual stimuli. In particular, we

207 found that neurons within deep layers conveyed more information than superficial neurons
208 about the planning of saccadic eye movements. These results suggest a division of labor
209 between superficial and deep layer neurons in the feedforward processing of stimulus features
210 and the application of sensory information to behavior.

211

212

213 **Methods**

214 **Subjects, Behavioral task, Visual Stimuli and Neuronal Recordings**

215 Details of the subjects, the task, the stimuli and recording techniques are described in ¹². In
216 brief, two male rhesus macaques were surgically implanted with recording chambers. Monkeys
217 were trained on an attention task that dissociated covert attention from saccade preparation.
218 Trials were initiated when the monkey fixated a central point. After 100 ms of central fixation, a
219 300-500ms “stimulus epoch,” occurred, where four oriented Gabor patches appeared at four
220 locations equidistant from the fixation point. This was followed by the “cue epoch,” lasting 600-
221 2,200 ms. During this epoch, a line appeared near the central fixation point, directed toward one
222 of the Gabor patches, indicating that it would potentially change orientations. After a variable
223 interval, the array of stimuli disappeared briefly (270 ms) and then reappeared. Monkeys were
224 trained to detect changes in orientation of any of the four stimuli upon reappearance. To
225 dissociate the direction of covert attention from that of saccade preparation, monkeys were
226 given a reward for responding to an orientation change with a saccade to the stimulus opposite
227 the changed stimulus (i.e. antisaccade). If no change occurred at the cued location (50% of
228 trials), the monkey was rewarded for maintaining fixation. Monkey G correctly responding on
229 69% of trials (77%, change trials; 62%, catch trials) and Monkey B correctly responding on 67%
230 of trials, (62%, change trials; 70%, catch trials).

231 Electrophysiological recordings were made from area V4 on the surface of the prelunate
232 gyrus with 16-channel, linear array U-Probes (Plexon, Inc., Dallas, TX). Electrodes were
233 cylindrical in shape (180 μ m diameter) with a row of 16 circular platinum/iridium electrical
234 contacts (15 μ m diameter) at 150 μ m center-to-center spacing (total length of array = 2.25 mm).
235 Recorded waveforms were classified as either “single neurons,” (277) or multi-neuron clusters
236 (421). We use “units,” to refer to activity of both types.

237

238 **Cortical Column Laminar Recordings**

239

240 ***Electrode targeting: Use of MRI guidance to achieve perpendicularity***

241 We sought to achieve simultaneous recordings at sites located within a single cortical "column."
242 In particular, the topographic organization of extrastriate visual cortex suggests that vertically
243 separated neurons should have overlapping RFs, so we sought to record from a column
244 principally by this definition. Since the cortical magnification factor (an estimate of how much
245 cortical tissue corresponds to units of retinal space) is approximately 1 deg/mm^{38} , we could
246 measure the approximate angle with the cortex by the distance between receptive fields
247 measured on the deepest and most superficial recording contacts, and sought to keep this
248 angle at 10 degrees or less, corresponding to a RF shift of ~ 0.5 degrees, given 2 mm thickness
249 of cortex.

250 In order to achieve these perpendicular penetrations we employed an MRI targeting
251 technique³⁹. We implanted the monkeys with custom built recording chambers made from
252 PEEK-type plastic, rather than from titanium, to avoid "shadows" in the MRI images. While we
253 did not employ ceramic skull screws, we took some care to ensure that the titanium skull screws
254 and plates were not located close to the recording chamber and brain areas of interest. We filled
255 a custom-made plastic cylinder with copper sulfate solution. We anesthetized the monkey and
256 inserted this cylinder into the recording chamber, into which it fit snugly. We performed
257 structural MRI imaging (1.5 Tesla; T-1 weighted image) to visualize the location and orientation
258 of the recording chamber (visible due to the high-contrast copper sulfate solution within it)
259 relative to the position of the prelunate gyrus within the brain. By manually identifying the
260 contours of the prelunate gyrus, we could compute perpendicular vectors to it and project these
261 back to the level of the electrode stage, thus identifying which penetration approach vectors
262 were likely to yield perpendicular penetrations.

263

264 ***Achieving desired approach vectors***

265 We employed a custom-built targeting device to angle and rotate the electrode into any desired
266 orientation and position in three dimensions. The device consisted of a “double-eccentric”
267 mechanism for positioning the electrode in the x-y plane of the well, a tilting mechanism, and a
268 rotating mechanism. All four coordinates could be set with sub- millimeter precision using
269 notches engraved in the device. The V4 recording chambers on both monkeys projected from
270 the monkeys’ heads at an angle such that there was a unique point on the chamber’s perimeter
271 at the lowest elevation. This point was identified computationally in the MRI images and was
272 identified on the chamber itself by filling the chamber with saline solution until the liquid first
273 contacted the lip of the chamber. With this point of alignment between the MRI images and the
274 physical well, the exact X, Y, tilt, and rotation coordinates for an approach vector specified by
275 the MRI images were geometrically determined.

276

277 ***Electrode targeting: Assessing perpendicularity with RF overlap***

278 RF positions and extents were estimated by computing the number of multi-unit spikes recorded
279 on each channel in the 200ms period following stimulus onset for each of probe location in a
280 RF-mapping task. During this task, subjects fixated a small (~0.3 d.v.a.) white dot against a
281 medium gray background. On each trial the six flash positions were selected from one of the
282 rows of the grid in random order. A horizontally oriented grating was flashed for 50 ms at each
283 position, with a 150-250ms variable delay between flashes. The flashes occurred at a total of 36
284 locations on a 6x6 grid with 3 d.v.a. spacing (total coverage 15x15 d.v.a.). If the subject
285 maintained fixation within a 1.8 d.v.a. square window until after the sixth flash, he received a
286 juice reward.

287 The upper right position of the grid was at the fovea such that only the lower left visual
288 field was covered by the mapping. This 6x6 matrix of response counts was cubic spline
289 interpolated to produce the full “RF map” and a 75%-of-max contour was determined, defining

290 the RF border. The center of mass of the portion of the RF map within the RF border was
291 defined as the RF center. This analysis was performed after recording RF-mapping task
292 responses but before the change-detection task, so that a stimulus position could be chosen at
293 a location that fell within the RF borders for all channels. If such a position was found, the
294 recording was included in further analyses.

295

296 ***Electrode targeting: Depth alignment***

297 We lowered electrodes into the brain rapidly ($\sim 25\mu\text{m}/\text{sec}$) until one channel was in the cortex,
298 based on visual examination of LFP and spiking activity being recorded concurrently. Then we
299 advanced the electrode slowly ($\sim 5\mu\text{m}/\text{sec}$) until the uppermost electrode contact was near the
300 point of entering the brain, being recorded during advancement. We withdrew the electrode
301 $500\mu\text{m}$ to release compression of the brain caused by the electrode. During this brief
302 withdrawal, no apparent change in the LFP or spiking activity was observed, confirming that this
303 served to relax the cortex rather than change the position of the electrode relative to the brain.
304 This manipulation qualitatively improved stability and recording quality. After reaching this
305 position, the full-field flash task was run to assess the depth.

306 During the full-field flash task, monkeys fixated a small (~ 0.3 d.v.a.) white dot against a
307 black background. The monitor turned maximal white for one frame ($\sim 8\text{ms}$) then back to black.
308 The flash occurred six times per trial with variable delays in the range of 150-250ms. If the
309 monkey maintained fixation within a 1.8 d.v.a. square window until after the sixth flash, he
310 received a juice reward. Approximately 30 trials, or 180 flashes, were completed per day. We
311 computed the current source density (CSD) response to the full-field flashes. The CSD reflects
312 the spatial and temporal position of current sources and sinks (i.e. where current flows into and
313 out of the extracellular space, respectively) along the length of the electrode, given certain
314 assumptions likely to be true for our recordings (Mitzdorf, 1985). The CSD can be computed
315 discretely as the second spatial derivative of the LFP for each point in time, that is:

316

$$D(z) = \frac{\phi(z+h) - 2\phi(z) + \phi(z-h)}{h^2}$$

317

318 where z is the position in depth, h is the distance between potential measurements (in
319 our case, 150 μ m), and $\phi(z)$ is the potential measured as a function of depth. We also
320 calculated the CSD according to the inverse estimation method⁴⁰, and display the results of this
321 calculation, which produces smoother, higher resolution plots of CSD, in figures for clarity.
322 However, results were qualitatively indistinguishable with both methods. Borders between
323 current sinks of interest were manually identified and channel depths were computed, in mm,
324 relative to these borders.

325

326 ***Depth registration***

327 In all included recordings, a prominent current sink was identified near the middle of the
328 electrode, approximately 40-50ms after flash onset. This was often followed by another sink just
329 below the first, peaking approximately 100ms after flash onset. These two sinks appeared in
330 every included recording, and we therefore aligned the recordings on these functional markers
331 of cortical laminae. In many recordings, further sinks were observed near the top of the probe at
332 ~150ms and near the bottom of the probe at ~50ms. Because the widths of all four of these
333 sinks, when present, were highly consistent from recording to recording, we assigned each
334 channel a depth relative to this central feature.

335 Depths were measured in millimeters, and positive depths indicate channels superficial
336 relative to the CSD feature. In some sessions, further CSD recordings at deeper locations
337 revealed that no further current sources or sinks of comparable magnitude could be identified
338 below these CSD features, assuring us that our electrode covered the depth of cortex. Two
339 alignments of these functionally defined layers with anatomical cortical layers seem possible.

340 The uppermost sink could correspond to layer 2/3 (together), and the larger sink to layer 4
341 (Figure 1c). Alternately, the four visible sinks could correspond to layer 2, 3, 4, and 5 in order
342 from superficial to deep. On the one hand, the first assignment seems reasonable as the
343 thickness of the layers known histologically matches the thickness of these CSD features
344 reasonably well, and our expectation from primary sensory areas is that layers 4 and 6 will have
345 the earliest responses⁴¹⁻⁴³. However, the cortex may well be compressed around the electrode
346 as it is inserted thus skewing the measured layer thicknesses. Layer 2 and 3 are well-
347 differentiated cytoarchitecturally in V4 unlike in V1, suggesting they may not appear as a single
348 sink. Furthermore, the earliest driving visual inputs into V4 are probably not from the ventral
349 stream⁴⁴, which project into layer 4¹⁵, and may instead arrive from the pulvinar nucleus of the
350 thalamus^{45,46}, which synapses into deep layer 3⁴⁷ (Jones, 2007). This would indicate that the
351 lower sink may correspond with the N95 marker used in previous studies to identify the granular
352 layer^{42,48-50}.

353

354

355 **Data Analysis**

356

357 ***Tuning and Modulation Indices***

358 To determine the tuning of each single neuron, we calculated the firing rate on each trial during
359 a 300ms block, from 50ms to 350ms relative to stimulus onset. We then labeled the trials by
360 stimulus orientation, and used a Kruskal-Wallis test to compare orientation distributions. If the
361 $p < 0.001$, we categorized the neuron as tuned. We then used a Chi-squared test to compare the
362 proportion tuned in superficial versus deep layers. We also fit a Gaussian tuning function to the
363 each neurons average firing rate for the eight stimuli using parameters for amplitude (a),
364 preferred orientation (b), width (c) and baseline (d). The formula was given by:

365

$$r(\theta) = a \times e^{-((\theta-b)/c)^2} + d$$

366

367 To obtain the parameters and goodness of fit measures, we used the Matlab fit function with
368 nonlinear least squares, and constraints of 0 for the lower bound of all variables, and an upper
369 bound of π for b and 8 for c . To determine if the neuron was well fit by the function, we used an
370 adjusted R^2 cutoff of 0.70. For each neuron, the averaged firing rates were rotated around π
371 until the optimal fit was achieved. We then compared the function parameters of superficial and
372 deep layer neurons. As the sample sizes of superficial and deep neurons were unequal, we
373 used bootstrapping without replacement to match the sample sizes, and repeated each test
374 1000 times. The reported p-values are the mean of those produced by a Wilcoxon signed-rank
375 test.

376

377 **Attention Modulation**

378 For each neuronal unit, we calculated the mean firing rate during the cue epoch from -500ms to
379 0ms relative to the blank period. For each unit, we then calculated the attention modulation
380 indices for eye movement preparation and covert attention relative to the orthogonal control,
381 using the standard formula:

382

$$Modulation\ Index = \frac{Attention - Orthogonal}{Attention + Orthogonal}$$

383

384 We then used a mixed effects model with fixed effects for neural depth, attention condition and
385 an interaction term (implemented with the R package nlme⁵¹). To make layer comparisons
386 within this omnibus model, we used three orthogonal contrasts: superficial attention conditions,
387 deep attention conditions and superficial neuronal units versus deep neuronal units. In all tests,
388 we included a random intercept for each neuronal unit, to control for repeat measures.

389

390 **Stimulus and Attention Classification**

391 ***Feature Matrix***

392 We assembled a dataset composed of neuronal firing rates recorded across the columnar
393 arrays and across multiple experimental sessions (23 sessions from Monkey G; 20 sessions
394 from Monkey B; 86 superficial neurons; 181 deep neurons) for all units for which we recorded a
395 minimum number of trials per orientation (20), or attention condition (200). Each column of the
396 feature matrix was a specific neuron's firing rate, and each row of that column was the neuron's
397 firing rate on a specific trial. The rows of each column were aligned, so that they shared the
398 same label for orientation or attention condition (depending on the epoch). The number of rows
399 associated with each orientation or attention condition were matched, so that chance level was
400 12.5% for the orientation epoch and 33% for the cue epoch. Each neuronal unit had multiple
401 columns in the feature matrix, corresponding to the number of bins in which firing rates were
402 calculated. The firing rates for the orientation and cue epochs were calculated in two 150ms
403 time bins, from 50ms following stimulus onset to 350ms following stimulus onset. This provided
404 a gross temporal pattern which was noted to improve performance in Nandy et al. (2016)²⁴.
405 When building feature matrices with variable population sizes, we randomly sampled a
406 population that size from all available units. This process was repeated 100 times, generating a
407 unique of feature matrix for each run of the decoder.

408

409 ***Random Forest Classification***

410 We used a Random Forest decoder, similar to that used in Nandy et al. (2016)²⁴, as
411 implemented by Matlabs (Mathworks TM) treebagger function. In addition to decoding based on
412 firing rate, Random Forest can decode based on differences in firing rate variability, even when
413 mean firing rates are equal^{52,53}. Furthermore, rather than comparing each orientation to the
414 others in turn, the decoder simultaneously considers all orientations. The decoder's decision

415 trees were trained on bags of trials (matrix rows), selected through bootstrapping with
416 replacement, and tested each decision tree on trials not included in the training bag. This out-of-
417 bag (OOB) error was used as the performance measure. It is significantly more conservative
418 than cross validation, but has the advantage of using all available data when training the
419 decoder. Furthermore, the bootstrapped sampling method has the traditional advantages
420 associated with bootstrapping, such as revealing the true underlying distribution from the
421 available training data, and reducing the impact of outlier trials⁵³. The decoder then used a
422 boosting method to create decision trees. At each branch point, a random subset of the features
423 (square root of the total number of features) was chosen to calculate potential decision
424 boundaries. Each of the features in the subset was used as a linear threshold for linearly
425 partitioning the population of trials. The Gini impurity (GI) of the original sample, as well as of
426 the two partitions was calculated using the formula:

$$GI = 1 - \sum_{i=1}^J p_i$$

427
428 Where J is the number of classes, and p_i is the probability of choosing stimulus class i at
429 random from the sample. The GI of the two partitions was averaged, and subtracted from the GI
430 of the parent sample. The feature with the greatest decrease in GI was used at the decision
431 boundary at that branch point. The use of a random subset of features reduces the influence of
432 outlier features, allowing one to be less careful about the neurons selected for use in decoding.
433 Stopping criteria for the decision trees was when either all the trials at a branch point had the
434 same label (GI = 0), or there were only 5 trials at the branch point. We set the number of trees
435 to 500. The decoder was trained and tested using each of the 100 feature matrices, producing a
436 distribution of decoder performance.

437 For visualization, we calculated the proximity matrix based on shared decision leaves,
438 and plotted the first two principal components for each trial.

439

440 ***Neuron-dropping Curves***

441 We used neuron-dropping curves to assess the performance of the decoder. Also known as
442 learning-curves, these are a standard tool in the machine learning to assess whether
443 performance limitations are due to the decoder, or to the quantity of data. When computing
444 these functions, the quantity of data used for decoding is varied and an error rate (or
445 performance level) is plotted as a function of that quantity. The presence of an asymptote
446 indicates that the decoder has reached maximal performance, whereas the absence of an
447 asymptote indicates more data is needed. We then fit a saturating function and compared both
448 the rate of rise, and the asymptotic value between populations.

449 We created pseudo-populations, starting with 5 units, and then incrementing by 5 until
450 the maximal number of available units was reached. For each population size, we randomly
451 sampled the requisite number from the larger population with replacement, repeating this
452 process 100 times to bootstrap a representative distribution. To this range of performance
453 levels, we fit the saturating function,

$$454 \quad f(s) = a \times e^{(-b \times s)} + c,$$

455 where s is the size of the population, a controls the y intercept, b the slope and c specifies the
456 function asymptote. This was implemented using the Matlab fit function with the method non-
457 linear least squares. A confidence interval of 95% was derived from the fitting process.

458

459

460

461 Citations

462

463 1. Felleman, D. J. & Van Essen, D. C. Distributed hierarchical processing in the primate cerebral
464 cortex. *Cereb. Cortex* **1**, 1–47 (1991).

465 2. Hilgetag, C. C., O’Neill, M. A. & Young, M. P. Indeterminate organization of the visual
466 system. *Science* **271**, 776–777 (1996).

467 3. Zeki, S. The distribution of wavelength and orientation selective cells in different areas of
468 monkey visual cortex. *Proc. R. Soc. Lond. B Biol. Sci.* **217**, 449–470 (1983).

469 4. Chang, M., Xian, S., Rubin, J. & Moore, T. Latency of chromatic information in area V4. *J.*
470 *Physiol. Paris* **108**, 11–17 (2014).

471 5. Desimone, R. & Schein, S. J. Visual properties of neurons in area V4 of the macaque:
472 sensitivity to stimulus form. *J. Neurophysiol.* **57**, 835–868 (1987).

473 6. Roe, A. W. *et al.* Toward a unified theory of visual area V4. *Neuron* **74**, 12–29 (2012).

474 7. Pasupathy, A. & Connor, C. E. Responses to contour features in macaque area V4. *J.*
475 *Neurophysiol.* **82**, 2490–2502 (1999).

476 8. Yau, J. M., Pasupathy, A., Brincat, S. L. & Connor, C. E. Curvature Processing Dynamics in
477 Macaque Area V4. *Cereb. Cortex* **23**, 198–209 (2013).

478 9. Tanigawa, H., Lu, H. D. & Roe, A. W. Functional organization for color and orientation in
479 macaque V4. *Nat. Neurosci.* **13**, 1542–1548 (2010).

480 10. Motter, B. C. Focal attention produces spatially selective processing in visual cortical areas
481 V1, V2, and V4 in the presence of competing stimuli. *J. Neurophysiol.* **70**, 909–919 (1993).

- 482 11. Baruni, J. K., Lau, B. & Salzman, C. D. Reward expectation differentially modulates
483 attentional behavior and activity in visual area V4. *Nat. Neurosci.* **18**, 1656–1663 (2015).
- 484 12. Steinmetz, N. A. & Moore, T. Eye movement preparation modulates neuronal responses in
485 area V4 when dissociated from attentional demands. *Neuron* **83**, 496–506 (2014).
- 486 13. Tolias, A. S. *et al.* Eye Movements Modulate Visual Receptive Fields of V4 Neurons. *Neuron*
487 **29**, 757–767 (2001).
- 488 14. Bichot, N. P., Rossi, A. F. & Desimone, R. Parallel and Serial Neural Mechanisms for Visual
489 Search in Macaque Area V4. *Science* **308**, 529–534 (2005).
- 490 15. Ungerleider, L. G., Galkin, T. W., Desimone, R. & Gattass, R. Cortical Connections of Area V4
491 in the Macaque. *Cereb. Cortex* **18**, 477–499 (2008).
- 492 16. Yukie, M. & Iwai, E. Laminar origin of direct projection from cortex area V1 to V4 in the
493 rhesus monkey. *Brain Res.* **346**, 383–386 (1985).
- 494 17. Nakamura, H., Gattass, R., Desimone, R. & Ungerleider, L. G. The modular organization of
495 projections from areas V1 and V2 to areas V4 and TEO in macaques. *J. Neurosci.* **13**, 3681–
496 3691 (1993).
- 497 18. Markov, N. T. *et al.* Anatomy of hierarchy: feedforward and feedback pathways in macaque
498 visual cortex. *J. Comp. Neurol.* **522**, 225–259 (2014).
- 499 19. Leichnetz, G. R., Spencer, R. F., Hardy, S. G. P. & Astruc, J. The prefrontal corticotectal
500 projection in the monkey; An anterograde and retrograde horseradish peroxidase study.
501 *Neuroscience* **6**, 1023–1041 (1981).

- 502 20. Gilbert, C. D. & Wiesel, T. N. Functional Organization of the Visual Cortex. in *Progress in*
503 *Brain Research* (eds. Changeux, J.-P., Glowinski, J., Imbert, M. & Bloom, F. E.) **58**, 209–218
504 (Elsevier, 1983).
- 505 21. Buffalo, E. A., Fries, P., Landman, R., Buschman, T. J. & Desimone, R. Laminar differences in
506 gamma and alpha coherence in the ventral stream. *Proc. Natl. Acad. Sci. U. S. A.* **108**,
507 11262–11267 (2011).
- 508 22. Nandy, A. S., Nassi, J. J. & Reynolds, J. H. Laminar organization of attentional modulation in
509 macaque visual area V4. *Neuron* **93**, 235–246 (2017).
- 510 23. Simons, D. J. & Rensink, R. A. Change blindness: past, present, and future. *Trends Cogn. Sci.*
511 **9**, 16–20 (2005).
- 512 24. Nandy, A. S., Mitchell, J. F., Jadi, M. P. & Reynolds, J. H. Neurons in Macaque Area V4 Are
513 Tuned for Complex Spatio-Temporal Patterns. *Neuron* **91**, 920–930 (2016).
- 514 25. Lebedev, M. A. How to read neuron-dropping curves? *Front. Syst. Neurosci.* **8**, (2014).
- 515 26. Bonhoeffer, T. & Grinvald, A. The layout of iso-orientation domains in area 18 of cat visual
516 cortex: optical imaging reveals a pinwheel-like organization. *J. Neurosci.* **13**, 4157–4180
517 (1993).
- 518 27. Fujita, I. & Fujita, T. Intrinsic connections in the macaque inferior temporal cortex. *J. Comp.*
519 *Neurol.* **368**, 467–486
- 520 28. Pasupathy, A. & Connor, C. E. Shape Representation in Area V4: Position-Specific Tuning for
521 Boundary Conformation. *J. Neurophysiol.* **86**, 2505–2519 (2001).
- 522 29. Kosai, Y., El-Shamayleh, Y., Fyall, A. M. & Pasupathy, A. The Role of Visual Area V4 in the
523 Discrimination of Partially Occluded Shapes. *J. Neurosci.* **34**, 8570–8584 (2014).

- 524 30. Moore, T., Tolias, A. S. & Schiller, P. H. Visual representations during saccadic eye
525 movements. *Proc. Natl. Acad. Sci.* **95**, 8981–8984 (1998).
- 526 31. Sheinberg, D. L. & Logothetis, N. K. Noticing Familiar Objects in Real World Scenes: The Role
527 of Temporal Cortical Neurons in Natural Vision. *J. Neurosci.* **21**, 1340–1350 (2001).
- 528 32. Reppas, J. B., Usrey, W. M. & Reid, R. C. Saccadic Eye Movements Modulate Visual
529 Responses in the Lateral Geniculate Nucleus. *Neuron* **35**, 961–974 (2002).
- 530 33. Bosman, C. A., Womelsdorf, T., Desimone, R. & Fries, P. A Microsaccadic Rhythm Modulates
531 Gamma-Band Synchronization and Behavior. *J. Neurosci.* **29**, 9471–9480 (2009).
- 532 34. Moore, T., Armstrong, K. M. & Fallah, M. Visuomotor origins of covert spatial attention.
533 *Neuron* **40**, 671–683 (2003).
- 534 35. Moore, T. Shape Representations and Visual Guidance of Saccadic Eye Movements. *Science*
535 **285**, 1914–1917 (1999).
- 536 36. Schafer, R. J. & Moore, T. Attention Governs Action in the Primate Frontal Eye Field. *Neuron*
537 **56**, 541–551 (2007).
- 538 37. Fries, W. Cortical projections to the superior colliculus in the macaque monkey: A
539 retrograde study using horseradish peroxidase. *J. Comp. Neurol.* **230**, 55–76
- 540 38. Gattass, R., Sousa, A. P. & Gross, C. G. Visuotopic organization and extent of V3 and V4 of
541 the macaque. *J. Neurosci.* **8**, 1831–1845 (1988).
- 542 39. Kalwani, R. M., Bloy, L., Elliott, M. A. & Gold, J. I. A method for localizing microelectrode
543 trajectories in the macaque brain using MRI. *J. Neurosci. Methods* **176**, 104–111 (2009).
- 544 40. Pettersen, K. H., Devor, A., Ulbert, I., Dale, A. M. & Einevoll, G. T. Current-source density
545 estimation based on inversion of electrostatic forward solution: Effects of finite extent of

- 546 neuronal activity and conductivity discontinuities. *J. Neurosci. Methods* **154**, 116–133
547 (2006).
- 548 41. Hansen, B. J. & Dragoi, V. Adaptation-induced synchronization in laminar cortical circuits.
549 *Proc. Natl. Acad. Sci.* **108**, 10720–10725 (2011).
- 550 42. Schroeder, C. E., Mehta, A. D. & Givre, S. J. A spatiotemporal profile of visual system
551 activation revealed by current source density analysis in the awake macaque. *Cereb. Cortex*
552 **8**, 575–592 (1998).
- 553 43. Swadlow, H. A., Gusev, A. G. & Bezdudnaya, T. Activation of a Cortical Column by a
554 Thalamocortical Impulse. *J. Neurosci.* **22**, 7766–7773 (2002).
- 555 44. Chen, C.-M. *et al.* Functional Anatomy and Interaction of Fast and Slow Visual Pathways in
556 Macaque Monkeys. *Cereb. Cortex* **17**, 1561–1569 (2007).
- 557 45. Guillery, R. W. & Sherman, S. M. Thalamic Relay Functions and Their Role in Corticocortical
558 Communication: Generalizations from the Visual System. *Neuron* **33**, 163–175 (2002).
- 559 46. Shipp, S. The functional logic of cortico–pulvinar connections. *Philos. Trans. R. Soc. Lond. B*
560 *Biol. Sci.* **358**, 1605–1624 (2003).
- 561 47. Edward G. Jones. *The thalamus*. (Springer Science+Business Media, LLC, Plenum Press,
562 1985).
- 563 48. Bollimunta, A., Chen, Y., Schroeder, C. E. & Ding, M. Neuronal Mechanisms of Cortical Alpha
564 Oscillations in Awake-Behaving Macaques. *J. Neurosci.* **28**, 9976–9988 (2008).
- 565 49. Givre, S. J., Schroeder, C. E. & Arezzo, J. C. Contribution of extrastriate area V4 to the
566 surface-recorded flash VEP in the awake macaque. *Vision Res.* **34**, 415–428 (1994).

- 567 50. Trongnetrpunya, A. *et al.* Assessing Granger Causality in Electrophysiological Data:
568 Removing the Adverse Effects of Common Signals via Bipolar Derivations. *Front. Syst.*
569 *Neurosci.* **9**, (2016).
- 570 51. Pinherio, J., Bates, D., DebRoy, S. & Sarkar, D. *nlme: Linear and Nonlinear Mixed Effects*
571 *Models.* (2018).
- 572 52. Strobl, C., Malley, J. & Tutz, G. An introduction to recursive partitioning: rationale,
573 application, and characteristics of classification and regression trees, bagging, and random
574 forests. *Psychol. Methods* **14**, 323 (2009).
- 575 53. Ho, T. K. A Data Complexity Analysis of Comparative Advantages of Decision Forest
576 Constructors. *Pattern Anal. Appl.* **5**, 102–112 (2002).
- 577
- 578

579 **Figure 1. Behavioral task and perpendicular recordings in area V4.** A) Panels depict phases of
580 the attention task, and lower left dashed circle denote RF position of recorded neurons, and
581 was not seen by subjects. Receptive fields of recorded neurons was always in the lower left, as
582 indicated by the dashed circle outline. Task began with fixation at a central fixation point.
583 Following fixation, randomly oriented Gabor gratings appeared at four positions. After an
584 additional period, a cue (white diagonal line) appeared near the fixation point and indicated
585 which grating was the target. A blank period followed in which the gratings disappeared, and
586 then the stimuli reappeared on the screen with the target presented either at the same
587 orientation or at a new orientation. Monkeys were rewarded for making saccadic eye
588 movements to the stimulus opposite the changed target (arrow) or for maintaining fixation
589 when the orientation did not change. B) Colored contours and corresponding dots respectively
590 show the RF borders and RF centers mapped at electrode channels across difference cortical
591 depths for an example V4 recording. C) Example current source density (CSD) with alignment
592 feature for the two monkey subjects. The delineation between superficial and deep layers is
593 indicated by the gray line.

594

595

596 **Figure 2. Orientation tuning in superficial and deep layers of area V4.** A) Left, distribution of
597 tuned units (red) among total units recorded (black) across cortical depth, relative to the
598 superficial/deep CSD border. Right, the same data plotted as a proportion. B) Average Gaussian
599 tuning fits, and definitions of fit parameters, for superficial (green) and deep (blue) neurons.
600 Line thicknesses denote \pm SEM. C) Left, performance of a Random Forest classifier at decoding

601 stimulus orientation across different population sizes of superficial (green) and deep blue)
602 neurons, along with shuffled controls for both (red and purple). Points indicate median values,
603 and bars indicate the SEM for the 100 decoder cycles at each size. Solid lines indicate the fit
604 saturating function. Right, multidimensional scaling (MDS) of classification for one cycle at the
605 maximum population size (210 neurons). Each color/shape combination is associated with a
606 unique orientation. Inset depicts the same MDS analysis after shuffling stimulus orientation
607 labels.

608

609 **Figure 3 Behavioral modulation in superficial and deep layers of V4.** A) Modulation indices
610 across cortical depth. Individual medians and SEMs are plotted at each depth for covert
611 attention (yellow) and saccade preparation (red), along with the total number of units recorded
612 (grey). Depths with fewer than five neurons were removed. B) Performance of Random Forest
613 decoder at distinguishing between the three behavioral conditions (covert attention, saccade
614 preparation or control) from superficial and deep neurons, as a function of neuronal population
615 size. C) Performance of the decoder at distinguishing between pairs of conditions: (top) saccade
616 preparation from control; (middle) saccade preparation from covert attention; (bottom) covert
617 attention from control.

618

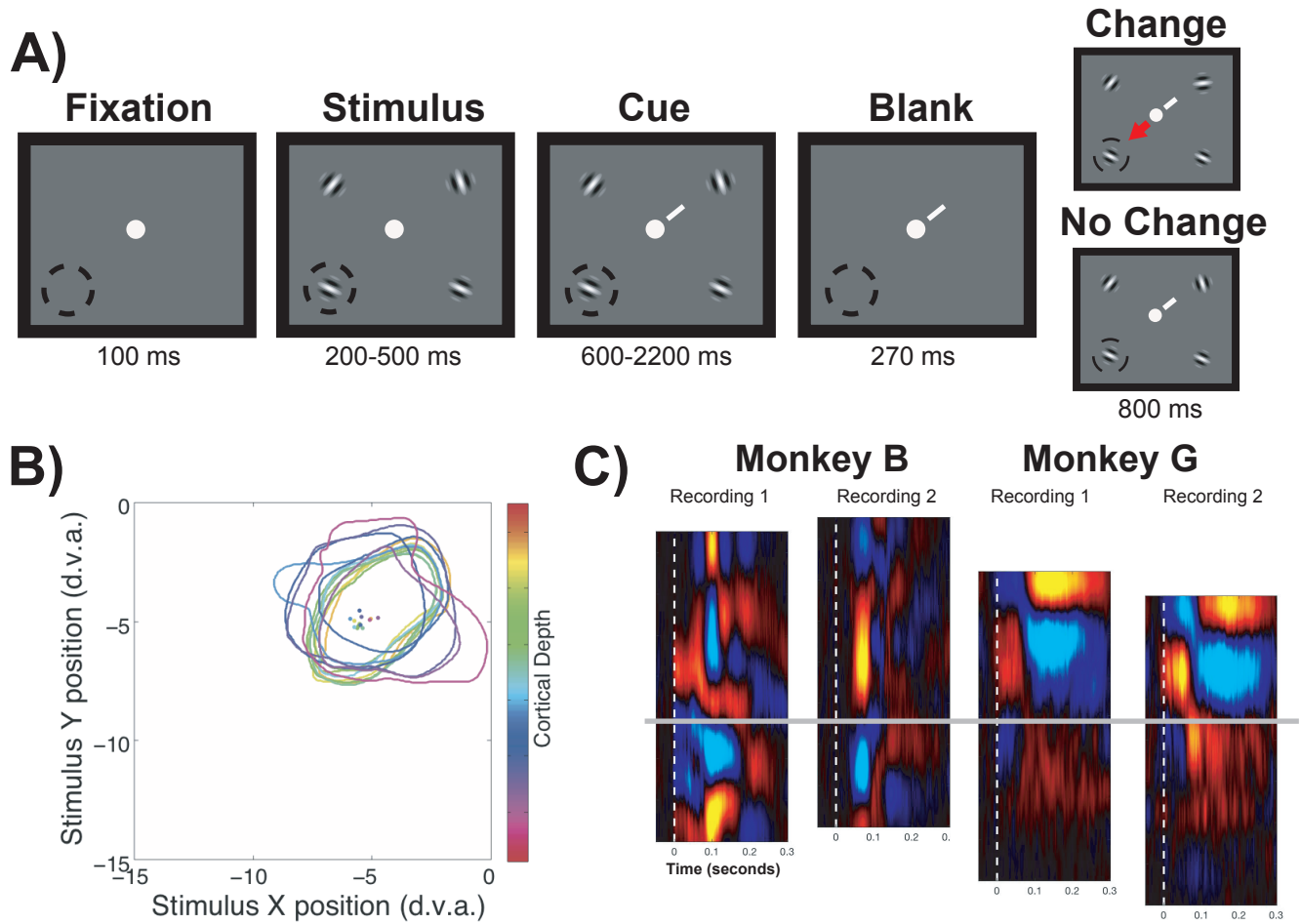


Figure 1
Pettine, Steinmetz and Moore

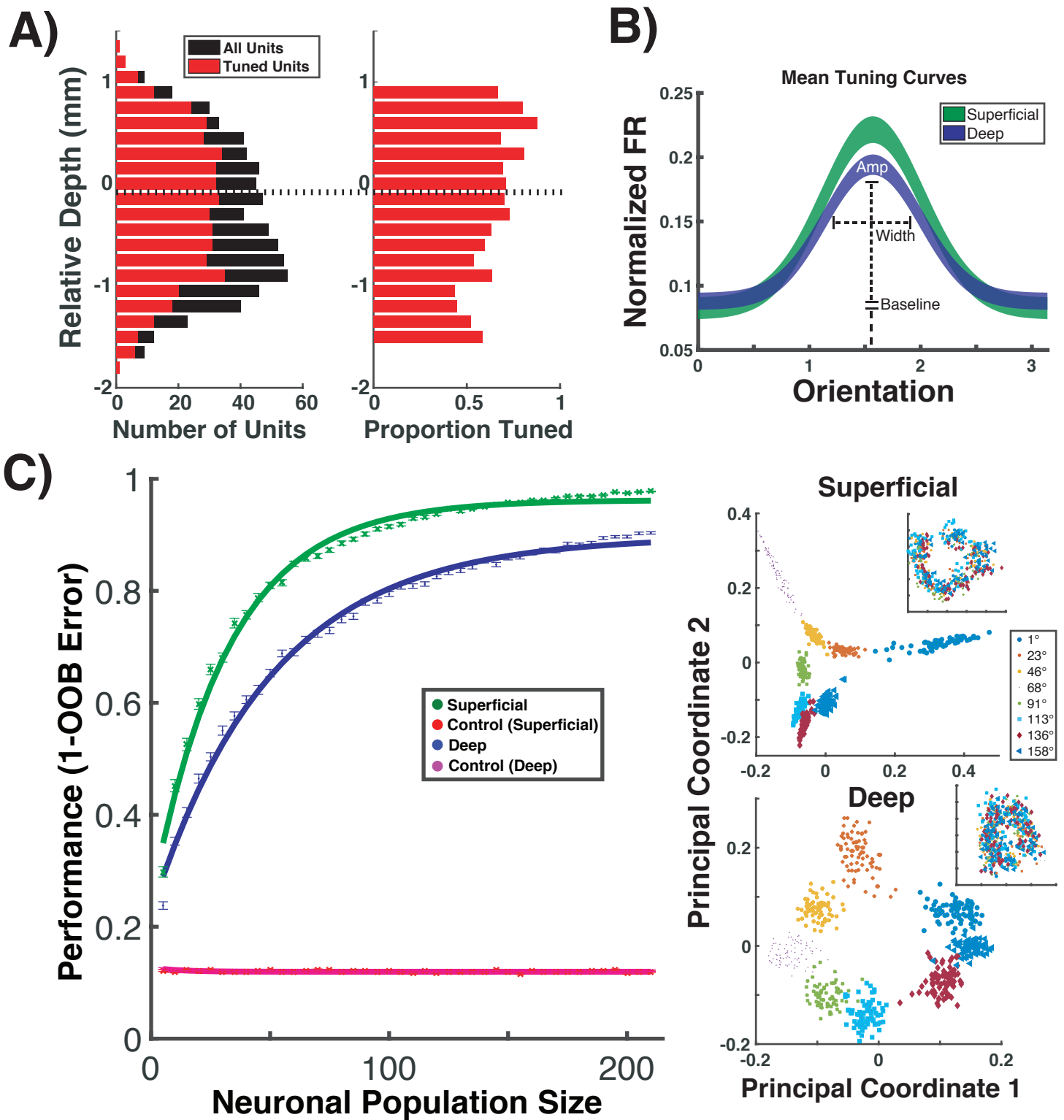


Figure 2

Pettine, Steinmetz and Moore

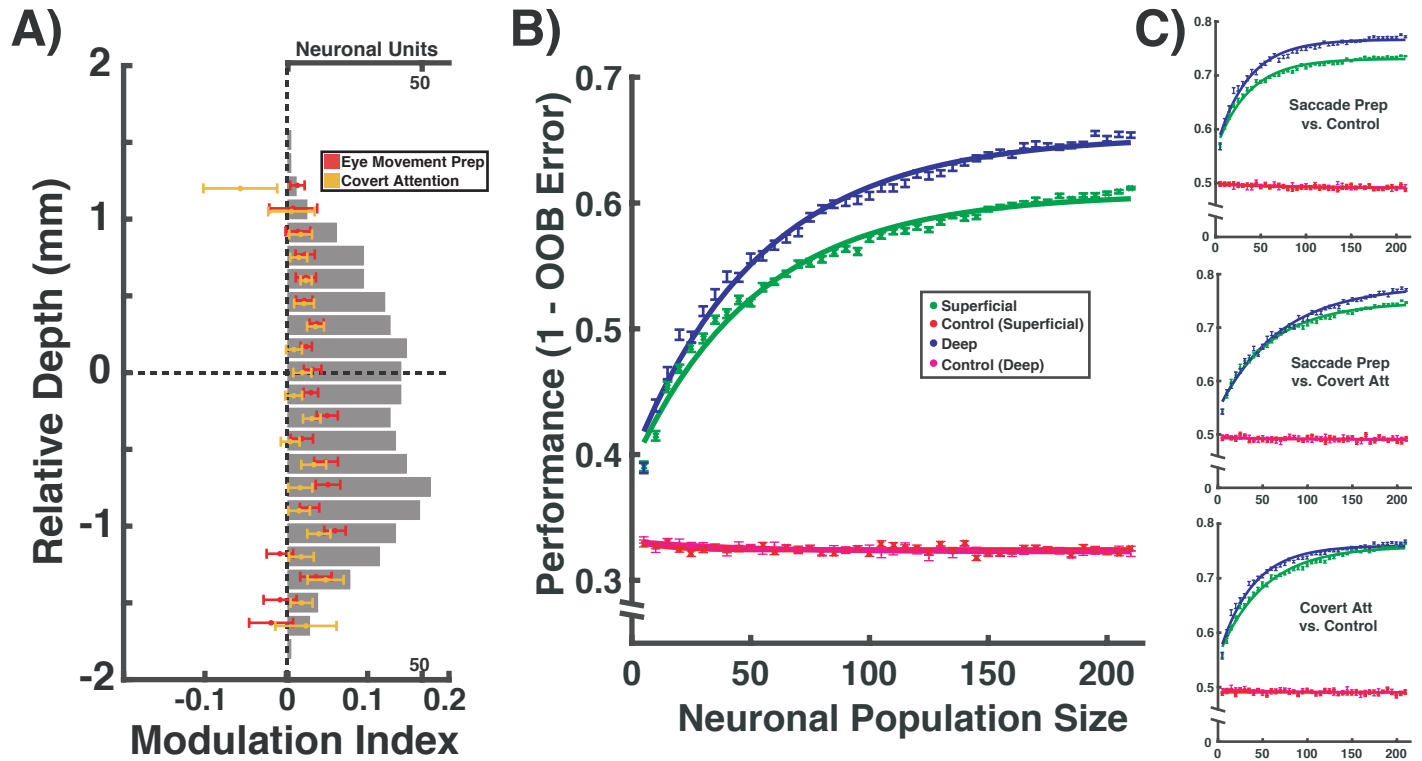


Figure 3
Pettine, Steinmetz and Moore